Available online at www.sciencedirect.com
ScienceDirect
International Journal of Heat and Mass Transfer 50 (2007) 3957–3965
International Journal of HEAT and MASS TRANSFER
www.elsevier.com/locate/ijhmt

Measurements on steady state heat transfer and flow structure and new correlations for heat and mass transfer in submerged impinging jets

Herbert Martin Hofmann *, Matthias Kind, Holger Martin

Institut für Thermische Verfahrenstechnik, Universität Karlsruhe (TH), Kaiserstr. 12, 76131 Karlsruhe, Germany

Available online 6 April 2007

Abstract

An experimental investigation on flow structure and heat transfer from a single round jet impinging perpendicularly on a flat plate has been performed. Heat transfer has been studied by means of thermography. The influence of nozzle-to-plate distance and Reynolds number on local heat transfer coefficient has been investigated. Based on the experimental results of this investigation as well as on experimental data from the literature, correlations for heat transfer coefficients have been developed. Similar correlations are presented for heat transfer between a two-dimensional impinging jet and a flat plate, based on literature data. Flow structure in a free jet has also been examined.

Keywords: Jet impingement; Velocity measurements; Heat transfer measurements; Slot nozzle; Round nozzle

1. Introduction

Impinging jets (Fig. 1) are widely used in technical applications, when high heat transfer coefficients are required. Therefore it is not surprising that this subject has been frequently treated in the past. Reviews on the subject may be found in Refs. [1–4]. The present work extends the investigations mentioned in these overviews by experiments with high spatial resolution, which cover the main factors influencing heat transfer of impinging jets. These experiments resulted in new correlations for improved prediction of local as well as surface-averaged Nusselt numbers for axisymmetric as well as for two-dimensional jets. This paper is part of a series, which covers investigation on jet impingement heat transfer for steady and pulsating jet flow.

2. Experimental setup

An experimental setup with an infrared sensitive camera for temperature measurements and a laser-doppler-velocimeter for velocity measurements was installed. The detailed description of the setup can be found in [5,6]. An air flow with preset mass flow rate and temperature is provided by an air supply system. It reaches the experimental chamber through a nozzle and impinges on a flat plate, which is heated on its reverse side. The flow structure is determined by velocity measurements in selected points. The local heat transfer coefficients are determined by means of the measurement of local temperatures on the surface of the plate. The experimental setup is presented schematically in Fig. 2.

2.1. Air supply

Air is provided by a blower (V1). The instant value of the mass flow is determined by a thermal mass flow meter (FIRC – 2 in Fig. 2). After the blower the energy dissipated by the blower is removed by a fin and tube heat exchanger

* Corresponding author. Present address: Behr GmbH & Co. KG, Siemensstr. 164, 70469 Stuttgart, Germany. Tel.: +49 711 896 10314; fax: +49 711 8902 10314.
E-mail address: herbert.hofmann@alumni.uni-karlsruhe.de (H.M. Hofmann).

0017-9310/$ - see front matter © 2007 Elsevier Ltd. All rights reserved.
doi:10.1016/j.ijheatmasstransfer.2007.01.023

Nomenclature

a	thermal diffusivity (m^2/s)
B	slot width (slot nozzle) (m)
D	nozzle diameter (round nozzle) (m)
H	nozzle-to-plate distance (m)
Nu	Nusselt number $\left(=\frac{\alpha D}{\lambda}\right)_{SRN}$, $\left(=\frac{\alpha S}{\lambda}\right)_{SSN}$
Pr	Prandtl number $\left(=\frac{\nu}{a}\right)$
r	radial distance from stagnation point (m)
S	hydraulic diameter of a slot nozzle ($=2B$)
Re	Reynolds number $\left(=\frac{uD}{\nu}\right)_{SRN}$, $\left(=\frac{uS}{\nu}\right)_{SSN}$
Sc	Schmidt number $\left(=\frac{\nu}{\delta}\right)$
Sh	Sherwood number $\left(=\frac{\beta D}{\delta}\right)_{SRN}$, $\left(=\frac{\beta S}{\delta}\right)_{SSN}$
T	temperature (K)
u	velocity component in axial direction (m/s)
x	horizontal distance from stagnation point (slot nozzle) (m)
z	axial distance from nozzle (m)

Greek symbols

α	heat transfer coefficient (based on $T_{Plate} - T_{Nozzle}$) (W/m^2 K)
β	mass transfer coefficient (analog to α) (m/s)
δ	diffusivity (m^2/s)
λ	thermal conductivity (W/(m K))
ν	kinematic viscosity (m^2/s)

Subscripts

N	normalized on jet exit velocity
SRN	single round nozzle
SSN	single slot nozzle

Superscripts

$'$	turbulent fluctuation of velocity component
$-$	mean value of velocity component

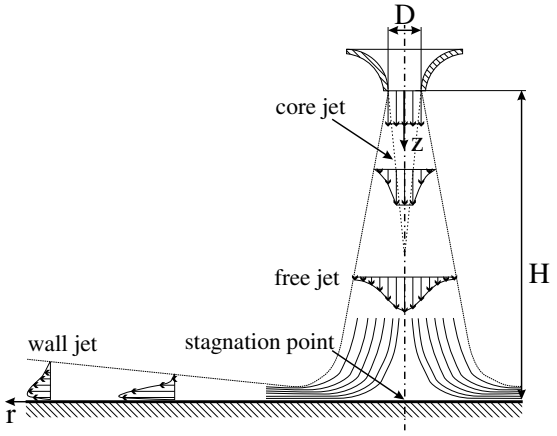

Fig. 1. Flow structure of an impinging jet.

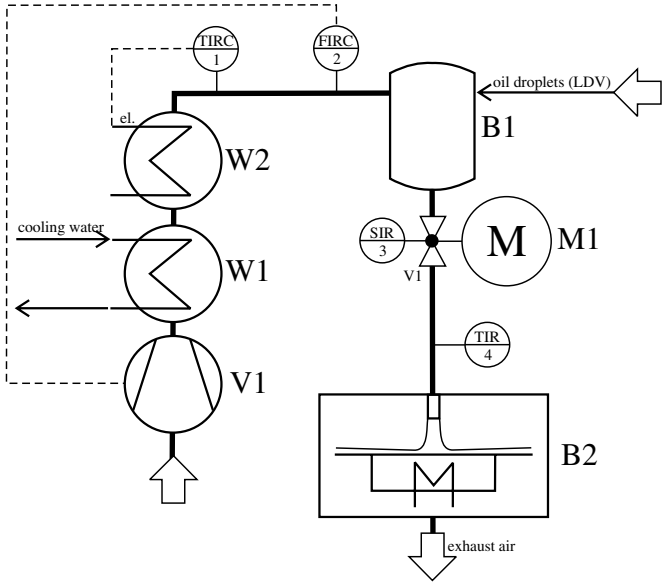

Fig. 2. Experimental setup.

(W1). To adjust the temperature an electric heater (W2) heats the air flow up to constant 30 °C. The vessel (B1) is used for injecting oil droplets, which are required for the velocity measurements. The oil fog is injected batchwise into the vessel, where the concentration of the oil droplets is reduced continuously by mixing with fresh air.

2.2. Experimental chamber

The experimental chamber is presented in Fig. 3. The air flow enters the experimental chamber through a nozzle with 25 mm diameter. The air flows from the nozzle into the experimental chamber and onto the plate. The position of the plate can be varied to provide nozzle-to-plate distances between 0.5 and 10 nozzle diameters. The bottom side of the plate is kept at constant temperature while the top side is cooled by the jet air. The local temperature values on the top side of the plate are measured by an infrared camera. Flow structure in the jet is determined by a laser-doppler-velocimeter. The experimental chamber is separated from the environment by a cylindrical casing to avoid uncontrolled entrainment of air from the environment into the jet. Its disadvantage is on the other side that the air in the experimental chamber is heated up by contact with the plate. Therefore the temperature of the environment and of the air entrained into the jet is slightly higher than the jet temperature.

According to measurements, performed by Striegl and Diller [7], an entrainment factor of $F = 0.8$ resulted for a jet with nozzle-to-plate spacing of 7 nozzle diameters in a heat transfer coefficient reduced by 20%. According to Martin [1] the entrainment factor is defined as

$$F = \frac{T_{Nozzle} - T_{Ambient}}{T_{Nozzle} - T_{Wall}}. \quad (1)$$

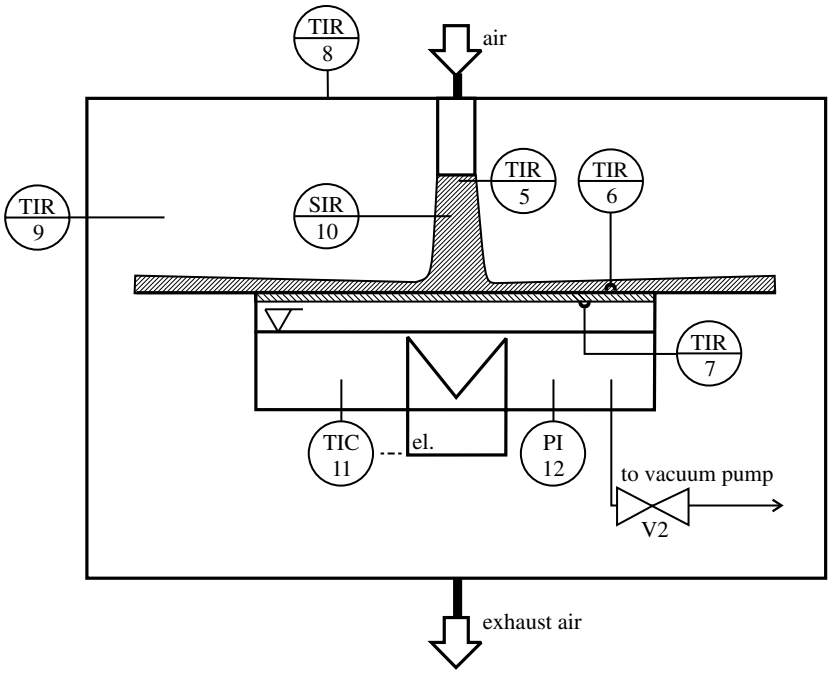

Fig. 3. Experimental chamber (B2) in detail.

In the present experiments the temperature of the ambient was recorded as 0.5–3 K above the jet temperature, resulting in entrainment factors of

$$F < 0.1 \tag{2}$$

in all cases. Therefore the effect of entrainment could be ignored. The casing was designed to 33 times the nozzle diameter in its height and diameter. Initial CFD calculations showed that at these dimensions no influence of the casing on the flow field near the stagnation point can be observed. The casing is open at its bottom and has a rectangular opening to enable the temperature measurements with the infrared camera. The impingement plate is the cap of a cylindrical vessel with electrical heaters. The vessel is evacuated and contains a water-steam atmosphere. When the impingement plate is cooled by the jet steam condenses at its bottom side. Due to the high heat transfer coefficients of condensing steam the temperature at the bottom side of the plate is kept constant. This was controlled by four resistance thermometers. The impingement plate was a glass plate painted black from the top. The jet hits upon the plate and cools it. With the temperature gradient through the plate in vertical direction being a function of thickness and material properties of the plate, the heat flux through the plate and from the plate to the jet air can be calculated. The local heat transfer coefficients are determined from the temperature difference between initial jet temperature and local plate temperature. Fig. 4 illustrates this principle.

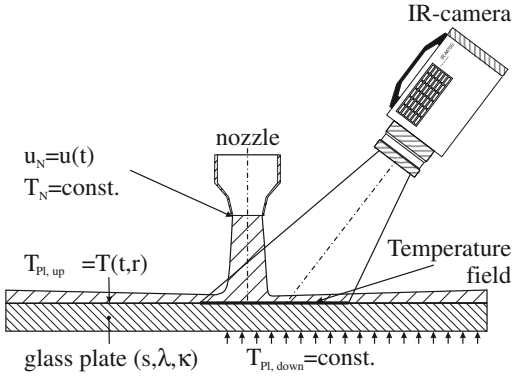

Fig. 4. Principle of heat transfer measurements.

3. Measurement principles

The infrared camera used for the experiments was a Mitsubishi M700 infrared camera, which records parts of the infrared radiation spectrum from the object, the camera is focused on. It calculates the temperature of the object from this information. This is performed for approximately 500×800 pixels per image.

The temperature fields both left and right from the stagnation point were recorded in 400 infrared images. After a calibration procedure, where the difference between local temperature of an isothermal plate measured with the infrared camera and local temperature of the plate measured with resistance thermometers was subtracted for each pixel, the temperature profiles along a line through the stagnation point were averaged over the time and gave a mean radial temperature profile.

The velocity measurements were performed with a TSI LaserVec Laser Doppler Velocimeter. This velocimeter was able to measure one velocity component. 100,000 data points were recorded and analyzed for one mean velocity and turbulence intensity value.

4. Flow measurements

As an initial step the flow structure of free and impinging jets were investigated. Fig. 5 shows the evolution of the mean axial velocity and the corresponding turbulence intensity with increasing distance from the nozzle for a Reynolds number of 78,000. Both values are normalized by the mean axial velocity at the nozzle exit. Immediately below the nozzle near plug flow is observed. The turbulence intensity is about 4%. In the boundary region turbulence intensity is increased due to high velocity gradients between the jet flow and the environment. With increasing axial distance from the nozzle the jet becomes broader and the core jet, where the initial conditions are still present, becomes smaller. In the regions, where entrainment takes place, turbulence is much higher than in the center of the jet. With increasing distance from the nozzle the turbulence level in the jet becomes more homogeneous and the velocity profile evolves into the typical free jet profile with a bell-shaped curve as it can be seen in Fig. 5. The left column shows the evolution of the mean axial velocity, divided by the mean velocity at the exit of the nozzle, where $\overline{u_N}$ stands for:

$$\overline{u_N} = \frac{\bar{u}}{\overline{u_{\text{Nozzle}}}} \tag{3}$$

while the right column shows the turbulence intensity, given in the following form:

$$\overline{u'_N} = \frac{\sqrt{\overline{u'^2}}}{\overline{u_{\text{Nozzle}}}}. \tag{4}$$

The core jet is clearly visible in the velocity and turbulence intensity profiles. The normalized turbulence intensity profile along the axis remains at its initial value up to a distance from the nozzle of $z/D = 4$.

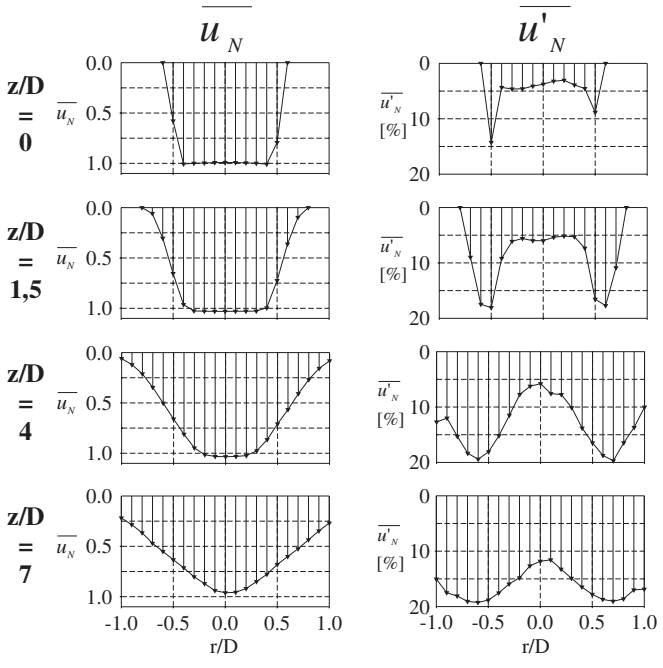

Fig. 5. Normalized axial velocity and turbulence intensity profiles in a free jets at different distances from the nozzle.

In a next step it was studied, how far these results can be applied to an impinging jet, too. Schrader [8] determined a distance of 1.2 nozzle diameters from the plate, above which free and impinging jets have the same flow structure. In the present examination a plate was placed at a distance of 2.5 nozzle diameters below the nozzle and the flow structure in axial direction at 1.5 nozzle diameters below the nozzle was measured and compared to the corresponding free jet experiments. The same comparison was performed for the flow structure at $z/D = 7$ with a plate placed at an axial distance of $H/D = 8$ from the nozzle. Fig. 6 shows a comparison of axial mean velocity and normalized turbulence intensity in a free jet and an impinging jet at a Reynolds number of 78,000. In mean velocity as well as in turbulence intensity the results are nearly the same. This means that even at an axial distance from the nozzle of 1 nozzle diameter, that is, at an even smaller value than determined by Schrader [8] no upstream influence of the plate on the flow structure was found.

5. Heat transfer measurements

5.1. Influence of flow conditions at the nozzle exit

To determine the influence of Reynolds number on heat transfer measurements at three different nozzle-to-plate distances were performed and the Reynolds number was varied over a wide range. At a distance of $H/D = 2.5$ the core jet is still present. The flow near the centerline has a low turbulence intensity and exhibits the characteristics of an ideal stagnation flow. The heat transfer coefficient (Fig. 7) starts in radial direction with a horizontal tangent and increases slightly, followed by a local minimum at $r/D \approx 1.2$ and by a maximum at $r/D \approx 2.2$. At larger radial distances the heat transfer coefficient decreases monotonically. The difference between the local minimum and the maximum increases with increasing Reynolds number. At small Reynolds numbers nearly no local extreme values – except the one at the stagnation point – are visible and the curve is similar to the curves at large nozzle-to-plate distances.

If the plate is placed at a distance of 5 nozzle diameters from the nozzle (Fig. 8) the core jet is not anymore present. At small Reynolds numbers the local maximum has already disappeared, while it is still present at larger Reynolds numbers. At a distance of 10 nozzle diameters between plate and nozzle the local Nusselt numbers are monotonically decreasing with increasing radial distance (r/D) (Fig. 9). This behavior is similar at different Reynolds numbers. The corresponding free jet shows at these distances a bell-shaped velocity profile and a homogeneous turbulence intensity profile. Local extreme values were not found at any one of the Reynolds numbers examined. Additional parameters, which influence heat transfer, are the velocity profile and the turbulence intensity of the flow

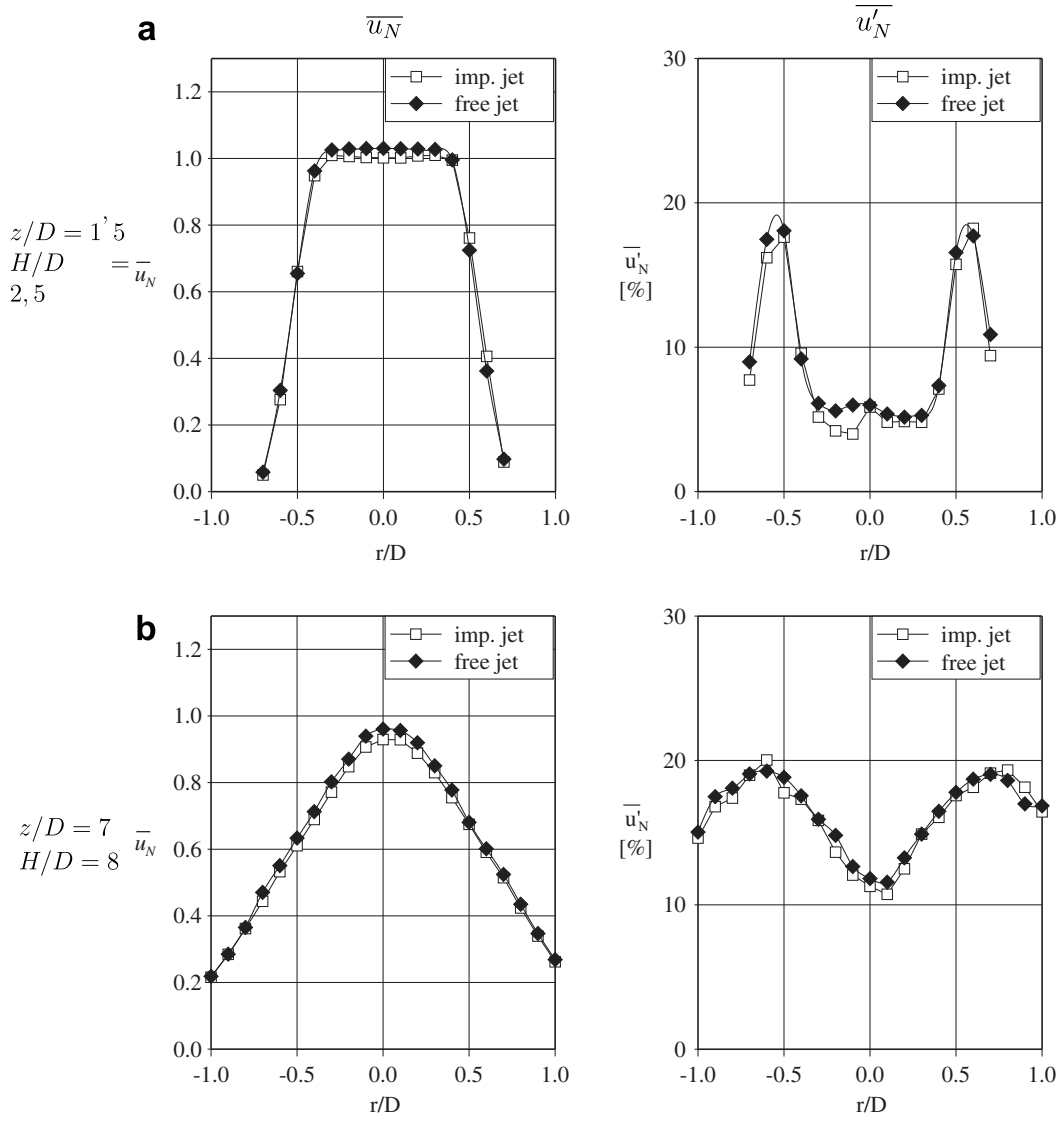

Fig. 6. Influence of an impingement plate on flow structure of a free jet at a distance of 1 nozzle diameter above the position of the plate ($Re = 78{,}000$).

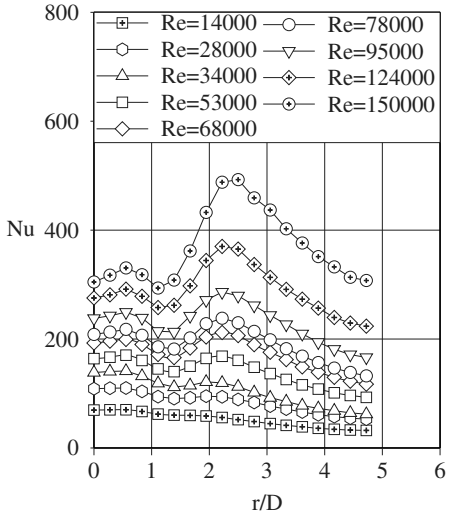

Fig. 7. Influence of Reynolds number on heat transfer at a nozzle-to-plate distance of 2.5 nozzle diameters.

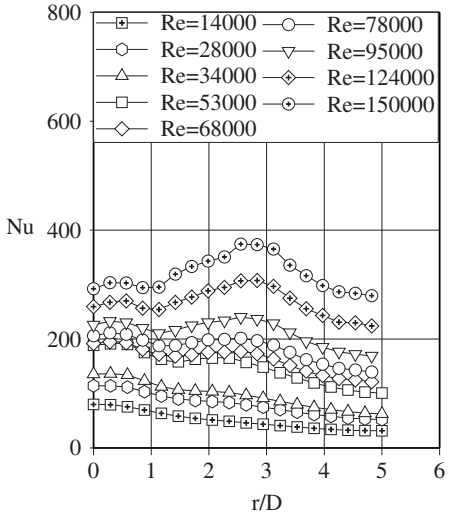

Fig. 8. Influence of Reynolds number on heat transfer coefficient at a nozzle-to-plate distance of 5 nozzle diameters.

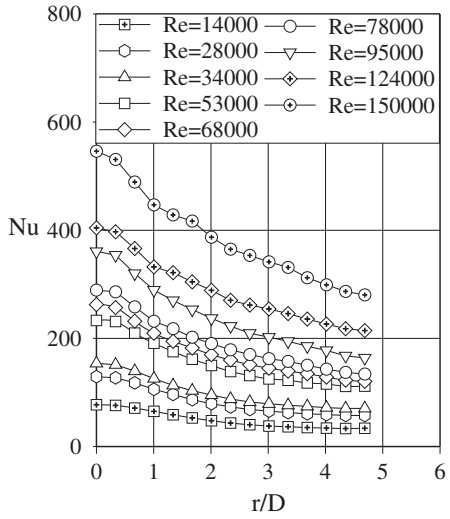

Fig. 9. Influence of Reynolds number on heat transfer coefficient at a nozzle-to-plate distance of 10 nozzle diameters.

at the nozzle. A metal screen (grid spacing 5 mm, wire diameter 1 mm) was fixed at the exit of the nozzle. The screen caused a strong increase in turbulence intensity as well as a change in the velocity profile. This change in velocity profile was caused by the holes near the wall of the nozzle, which were partly covered by the wall and had a larger flow resistance than the uncovered holes. Heat transfer was also influenced by the screen. In Fig. 10 temperature profiles at the top of the glass plate are shown at an undisturbed jet $H/D = 2$ (a) and with screen for different nozzle-to-plate distances (b–d). Even at the smallest distance ($H/D = 2$) no secondary maximum is visible. The temperature distribution is much more asymmetrical than

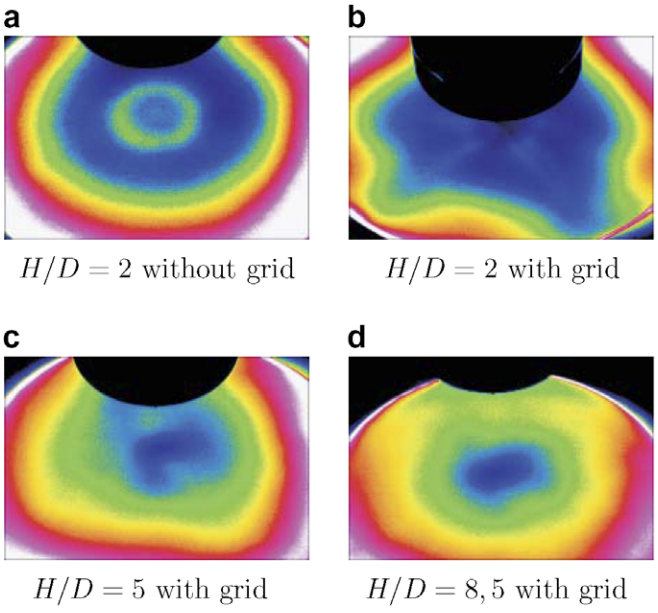

Fig. 10. Infrared images of an impingement plate to illustrate the influence of a coarse grid at the exit of the nozzle on heat transfer at different nozzle-to-plate distances ($Re = 78{,}000$).

in the undisturbed jet (a). The asymmetry disappears with increasing nozzle-to-plate distance, so that temperature distribution at larger nozzle-to-plate distances ($H/D = 5$ and $H/D = 8.5$) is much more symmetrical.

5.2. Influence of nozzle-to-plate distance

In Figs. 11–13 influence of nozzle-to-plate distance is shown for Reynolds numbers of $Re = 14{,}000$, $Re = 34{,}000$ and $Re = 78{,}000$, respectively. At large Reynolds numbers heat transfer near the stagnation point increases with increasing nozzle-to-plate distance over the whole range of distances examined. At small Reynolds numbers a decrease in heat transfer takes place already at a nozzle-to-plate distance of 8.5. The decrease in heat transfer coefficient in the region of local extreme values compensates this increase for surface-averaged heat transfer coeffi-

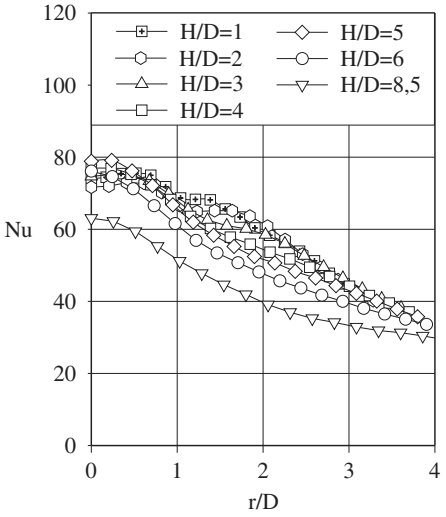

Fig. 11. Influence of nozzle-to-plate distance on heat transfer for $Re = 14{,}000$.

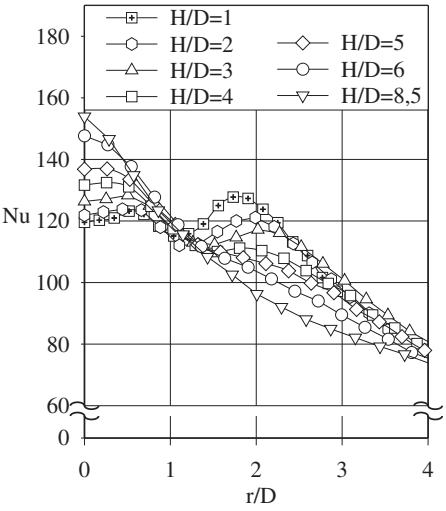

Fig. 12. Influence of nozzle-to-plate distance on heat transfer for $Re = 34{,}000$.

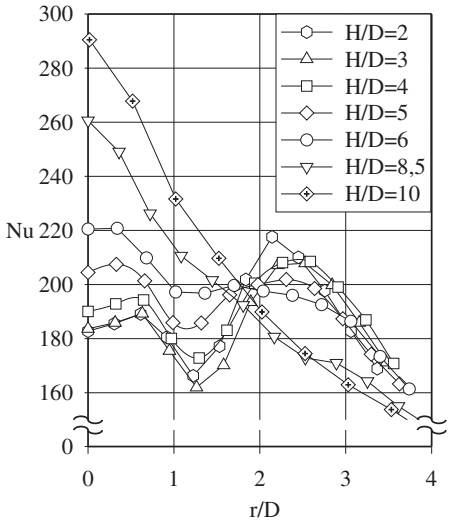

Fig. 13. Influence of nozzle-to-plate distance on heat transfer for $Re = 78{,}000$.

cients. But the diagrams make clear that depending on radial distance from the stagnation point, increasing nozzle-to-plate spacing can cause increase as well as decrease in heat transfer. Remarkable is that all curves come together at $r/D \approx 2$. Additionally it is remarkable, that nozzle-to-plate distance has only a small effect on heat transfer for large radial distances from the stagnation point. From these experiments it can be concluded that heat transfer depends on nozzle-to-plate spacing, but no simple relationship can be found to describe this influence on local heat transfer coefficients in a simple correlation. The reason is that varying nozzle-to-plate-spacing varies the heat transfer coefficients as well as their dependency on Reynolds number and radial distance from the stagnation point. Taking these effects into account would lead to a correlation too complex for practical applications. Therefore the influence of H/D was neglected in the correlations presented in the next section.

6. New correlations for jet impingement heat transfer

New correlations were developed, which fulfill the following requirements: The correlations have a simple form to be convenient for practical applications. They show no strong deviations from the experimental data from different authors – also near the stagnation point. As round jets and jets from slot nozzles are quite similar in their physical behavior, correlations for slot nozzles and for round nozzles have similar shape and predict the physically reasonable behavior, even when extrapolating the correlations. Correlations were developed to predict local heat transfer coefficients as well as surface-averaged heat transfer coefficients in agreement with the experimental data, given in [9,10], and in this work. The authors, whose data are used for this study had different measurement techniques: Adler [9] used an electrically heated foil and recorded the temperature distribution on the surface of the foil with an infrared camera. Weyl [10] measured water evaporation along clay rings.

After analyzing all the experimental data, it became clear that a simple function could predict the relationship between Nusselt number and Reynolds number. The dependency on radial distance from the stagnation point was predicted best with a Gaussian curve. The dependency of Nusselt number on Prandtl number for $Nu \propto Pr^{0.42}$ was adopted from [11]. This dependency was confirmed recently by Shi et al. [12], who performed numerical calculations with different fluids for axisymmetric jets. For predicting the influence of nozzle-to-plate distance no clear relationship could be found for the relatively small nozzle-to-plate-spacings, investigated in this work. As shown in Figs. 11–13 increasing nozzle-to-plate-spacing yields for small spacings to increasing heat transfer near the stagnation point and decreasing heat transfer in some distance to the stagnation point. The reason for this behavior is, that increasing nozzle-to-plate-spacing results in increasing jet width and therefore in smaller velocities near the wall, which reduce heat transfer. On the other side turbulence intensity increases, which has the opposite effect. This results in a complex relationship, where the influence of nozzle-to-plate-spacing has to be described with a function including turbulence intensity, Reynolds number and radial distance from the stagnation point. For describing these effects in detail the experimental basis has to be further extended.

The resulting correlation for local Nusselt numbers in axisymmetric jets has the following form:

$$Nu_{\mathrm{loc}} = 0.055[Re^3 + 10Re^2]^{0.25} \cdot Pr^{0.42} \cdot \mathrm{e}^{-0.025(r/D)^2}. \tag{5}$$

This correlation can easily be integrated and by that integration

$$Nu_{\mathrm{int}} = \frac{2}{r^2}\int_0^r Nu_{\mathrm{loc}} \cdot r\,\mathrm{d}r \tag{6}$$

the correlation for surface-averaged Nusselt numbers is explicitly obtained:

$$Nu_{\mathrm{int}} = Pr^{0.42}[Re^3 + 10Re^2]^{0.25} 0.055 \cdot \frac{1 - \mathrm{e}^{-0.025(r/D)^2}}{0.025(r/D)^2}. \tag{7}$$

Both equations are valid in the range of:

$$\begin{aligned} &14{,}000 < Re < 230{,}000, \\ &0.5 < H/D < 10, \\ &0 < r/D < 8. \end{aligned} \tag{8}$$

For a comparison the correlation of Schlünder and Gnielinksi [11], in the form, recommended by Martin [1] given in Eq. (9)

$$\left(\frac{Sh}{Sc^{0.42}}\right)_{\mathrm{SRN}} = \left(\frac{Nu}{Pr^{0.42}}\right)_{\mathrm{SRN}} = \frac{D}{r}\,\frac{1 - 1.1/(r/D)}{1 + 0.1(H/D - 6)/(r/D)} \cdot F(Re) \tag{9}$$

is differentiated by the radial distance and an equation for local heat or mass transfer coefficients is obtained:

$$\frac{Nu_{\mathrm{loc}}}{Pr^{0.42}} = \frac{D}{2r}\frac{1}{Pr^{0.42}}\frac{\partial\left(\left(\frac{r}{D}\right)^2 \cdot Nu_{\mathrm{int}}\right)}{\partial\left(\frac{r}{D}\right)} = 5 \cdot \frac{10\frac{r}{D} + 2\frac{H}{D} - 12 - 1.1\frac{D}{r}\left(\frac{H}{D}+6\right)}{\left(10\frac{r}{D}+\frac{H}{D}-6\right)^2} \cdot F(Re) \qquad (10)$$

with

$$F(Re) = 2[Re(1 + 0.005Re^{0.55})]^{0.5}. \qquad (11)$$

Eq. (10) was used together with the initial correlation for surface-averaged heat transfer coefficients for an assessment of the quality of the new correlation. Fig. 14 shows a comparison of experimental data from [11], where the Nusselt numbers were calculated from the Sherwood numbers given in this publication by the relationship

$$Nu = \left[\frac{Pr}{Sc}\right]^{0.42} Sh \qquad (12)$$

and own experimental data with the new correlation (Eq. (5)) and the local form of the correlation derived from [11] (Eq. (10)) at $H/D = 2.5$. It can be seen that the own experiments agree with Schluender's measurements in the wall jet region ($r/D > 2.5$). In the stagnation region the own experiments give lower heat transfer coefficients, which is probably caused by the smoother surface used in these experiments, compared to Schlünder's experimental setup. The correlation from [11] (Eq. (10)) shows an inconsistency near the stagnation point, due to its hyperbolic character. For larger radial distances it approaches the experimental data and the correlation from Eq. (5). The

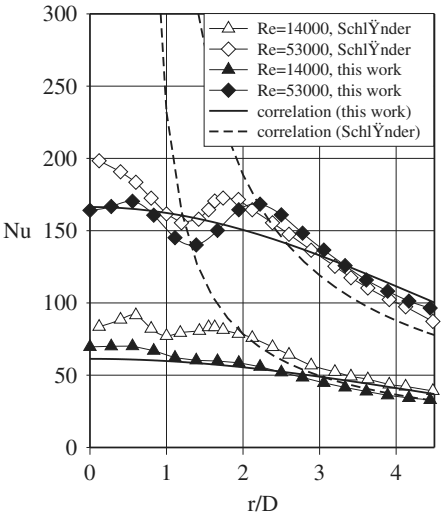

Fig. 14. Comparison of local Nusselt numbers at $H/D = 2.5$ from own experiments (black symbols) with Nusselt numbers calculated from Schlünder's experiments (white symbols) [11], the correlation from Eq. (5) (solid line) and a correlation for local Nusselt numbers derived from Schlünder's correlation [11] (dashed line).

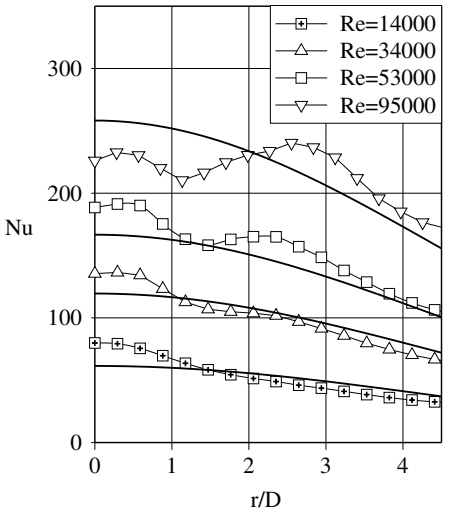

Fig. 15. Comparison of local Nusselt numbers from own experiments (symbols) and the correlation from Eq. (5) (lines) at $H/D = 5$ and different Reynolds numbers.

new correlation gives a good prediction for all radial distances.

The experimental data are predicted from Eqs. (5) and (7) with a standard deviation of 20% (local) and 16% (surface-averaged) better than with the correlation of [11]. Fig. 15 shows a comparison of local Nusselt numbers with the correlation at a nozzle-to-plate distance of $H/D = 5$. A good agreement between correlation and experimental data can be seen.

For two-dimensional jets a similar approximation was performed. For this geometry no own experiments were available. Therefore the development of the correlation was fit to literature data [13,10,14]. These data could be predicted satisfactorily with the following equation:

$$Nu_{\mathrm{loc}} = Pr^{0.42}[Re^3 + 10Re^2]^{0.25}0.042 \cdot \mathrm{e}^{-0.052(x/S)}, \qquad (13)$$

which yields the following equation for surface-averaged Nusselt numbers:

$$Nu_{\mathrm{int}} = Pr^{0.42}[Re^3 + 10Re^2]^{0.25} \cdot \frac{1 - \mathrm{e}^{-0.052(x/S)}}{1.24(x/S)}. \qquad (14)$$

The agreement for this data was not as good as for the axisymmetric jet, but the agreement is as good as for the correlation recommended by Martin [1] and for the equation for local Nusselt numbers derived from this correlation.

The correlation is valid for a range of:

$$\begin{aligned} &3000 < Re < 210,000, \\ &0.5 < H/S < 40, \\ &0 < x/S < 70. \end{aligned} \qquad (15)$$

7. Conclusions

New experiments on flow structure and heat transfer in the impinging jet have been performed, which show the complex interaction of nozzle-to-plate spacing, radial dis-

tance from the stagnation point and the Reynolds number. The influence of Reynolds number and radial distance from the stagnation point on heat transfer coefficient were described by a correlation, which is valid for predicting local and surface-averaged values of heat transfer coefficients. The correlation is in good agreement with experimental data of several authors.

Acknowledgements

The authors thank Mr. Andreas Daiss, Mr. Rafael Kaiser, Mr. Johann Siemens and Ms. Meirosalyna Prima for their contribution to this work.

References

[1] H. Martin, Heat and mass transfer between impinging gas jets and solid surfaces, Adv. Heat Transfer 13 (1977) 1–60.
[2] K. Jambunathan, E. Lai, M.A. Moss, B.L. Button, A review of heat transfer data for single circular jet impingement, Int. J. Heat Fluid Flow 13 (1992) 106–115.
[3] S. Polat, Heat and mass transfer in impingement drying, Drying Technol. 11 (1993) 1147–1176.
[4] R. Viskanta, Heat transfer to impinging isothermal gas and flame jets, Exp. Therm. Fluid Sci. 6 (1993) 111–134.
[5] H. Hofmann, Wärmeübergang beim pulsierenden Prallstrahl, Dissertation Universität Karlsruhe (TH), 2005.
[6] H. Hofmann, H. Martin, M. Kind, Experimental setup for heat transfer measurements in pulsating impinging jet flow, in: Proceedings of International Symposium on Transient Convective Heat and Mass Transfer in Single and Two-Phase Flows Cesme, Turkey, 2003, pp. 373–381.
[7] S.A. Striegl, T.E. Diller, The effect of entrainment temperature on jet impingement heat transfer, J. Heat Transfer 106 (1984) 27–33.
[8] H. Schrader, Trocknung feuchter Oberflächen mittels Warmluftstrahlen, vol. 484, VDI-Forschungsheft, 1966.
[9] W. Adler, Experimentelle Bestimmung des Wärmeübergangs bei der Prallströmung über einen hohen Reynoldszahlenbereich mittels Infrarot-Thermografie, Dissertation Otto-von-Guericke-Universität, Magdeburg, 2002.
[10] R. Weyl, Stoff- und Wärmeübergang bei Prallströmung aus Düsen, Diplomarbeit Max-Planck-Institut, Göttingen, 1969.
[11] E.-U. Schlünder, V. Gnielinksi, Wärme- und Stoffübergang zwischen Gut und aufprallendem Düsenstrahl, Chem.-Ing.-Tech. 39 (1967) 578–584.
[12] Y. Shi, M.B. Ray, A.S. Mujumdar, Effects of Prandtl number on impinging jet heat transfer under a semi-confined turbulent slot jet, Int. Commun. Heat Mass Transfer 29 (2002) 929–938.
[13] H.-M. Esche, Stoffübergang bei Prallströmung aus Schlitzdüsen, Diplomarbeit Max-Planck-Institut, Göttingen, 1968.
[14] H. Martin, Stoffübergang bei Prallströmung aus Schlitzdüsen und Düsenfeldern, Diplomarbeit Max-Planck-Institut, Göttingen, 1968.